

Low energy ion assisted deposition of Ta/Cu films

J. J. Quan^{a)}

Department of Engineering Physics, University of Virginia, Charlottesville, Virginia 22904

X. W. Zhou

Mechanics of Materials Department, Sandia National Laboratories, Livermore, California 94550

L. He, R. Hull, and H. N. G. Wadley

Department of Materials Science and Engineering, University of Virginia, Charlottesville, Virginia 22904

(Received 5 September 2006; accepted 11 November 2006; published online 23 January 2007)

A combination of molecular dynamics simulations and experiments has been used to investigate the use of various low energy ion assisted vapor deposition approaches for controlling the interfacial structures of a model copper/tantalum multilayer system. Films were grown using argon ion beam assistance with either a fixed or modulated ion energy during metal deposition. The effect of sequential ion assistance (after layer's deposition) was also investigated. The argon ion energy was varied between 0 and 50 eV and the effect on the atomic scale structure of Ta/Cu film interfaces and the film electrical resistivity were studied. The use of simultaneous argon ion assistance with an ion energy of ~ 10 eV and an ion/metal atom flux ratio of ~ 6 resulted in atomically sharp interfaces with little intermixing, consistent with simulation predictions. Ion impacts in this range activated surface atom jumping and promoted a step flow film growth mode. Higher energies were also successful at interface flattening, but they caused significant intermixing between the layers and increased film's resistivity. This could be reduced using modulated ion energy and sequential ion beam assistance. This was again consistent with atomic scale simulations, which indicated that metal layers deposited over an interface before ion assistance was initiated impeded atom exchange across interfaces and therefore intermixing. © 2007 American Institute of Physics.

[DOI: [10.1063/1.2430705](https://doi.org/10.1063/1.2430705)]

I. INTRODUCTION

Metal multilayers are widely used for x-ray mirrors, for magnetic data storage systems, and for microelectronic circuits and interconnects.¹ Device performance in all these applications is usually increased when the interfaces between the metal layers are atomically flat and chemically sharp.²⁻⁴ An atomically flat interface can only be created if the film surface of a previously deposited layer is already flat at the start of the deposition of the next layer. To fabricate devices like those identified above, a smooth buffer layer is first deposited on a semiconductor substrate. This is then followed by the controlled deposition of the metallic multilayer system of interest. The atomic scale flatness of the buffer layer surface and the structure of the interface between it and a subsequently deposited metal (especially intermixing) can significantly affect the magnetic properties and x-ray reflectivity of the deposited structures.^{5,6}

Ion assistance is a well known method for modifying film structures and properties.⁷ Inert gas ion bombardment improves the atomic structure (smoothness) of a surface and reduces the electrical resistance of the film by improving its atomic scale perfection as the film is grown.⁷ Two approaches can be used to create an assisting ion flux. One exploits ion beam sources, such as the Kaufman ion gun,^{8,9} to generate energetic ions that impact a substrate. Ion polishing is a well-established example of the use of this kind of

ion source.^{10,11} In this process, ions are accelerated in an ion beam gun up to several hundreds or thousands of eV. These ions then strike the film surface at an oblique angle and preferentially sputter the most weakly bound atoms from the surface (those with the fewest bonds to neighboring atoms). The surface then becomes smoother due to the preferential removal of material from convex areas of the surface. In "ion polishing," the energy of the ions is usually well above the sputtering threshold for the film. The ion energy threshold depends on the cohesive energy of the surface atoms and the fraction of the ions energy transferred to the surface atoms. For transition metals using argon ions, this is in the 50 eV range.^{12,13}

The second approach creates a plasma to which a negative bias voltage is applied between it and the substrate.^{7,14} The combination of the plasma potential and the applied bias accelerates the ions from the plasma toward the growth surface where they typically make impact with a near normal incidence angle. A low background pressure reduces ion energy loss by binary scattering but also reduces the ion flux. Magnetic fields are often then used to enhance the ion concentration. This magnetron sputtering method has been widely used for the deposition of single layer metal films.^{15,16} The deposition process can to some extent be optimized by modification of the negative substrate bias voltage. In the traditional single layer film deposition process, a high bias voltage of several hundred volts has been experimentally found to produce the smoothest films.⁷ Although ion impacts with an energy in the range of hundreds of eV

^{a)}Electronic mail: junjie.quan@gmail.com

lead to a significant reduction of surface roughness, such impacts can also create other defects and induce alloying at interfaces within multilayer structures.^{17,18} Higher pressure sputtering processes utilize binary ion-background gas atom collisions to reduce the ion impact energies and have been used for the growth of some metallic multilayers.¹⁹

Several experimental and molecular dynamics simulation studies indicate that even very low energy (a few eV) atom or ion impacts with a growth surface can result in defect creation and mixing at the interfaces in metal multilayers.^{17,18,20–22} These imperfections significantly affect thin film properties. For example, interlayer mixing in magnetic films creates a magnetic dead layer at the interface that degrades the performance of giant magnetoresistance multilayers.^{3,23} Amorphous layers formed by solid state alloying between Ta and Cu also affect the properties of interconnects.²⁴

Several groups have tried to explore low energy ion assisted deposition approaches and have shown significant ion assistance effects on thin film structures.²⁵ However, the atomic scale assembly mechanisms in this ion energy regime have not been extensively investigated and practical difficulties, such as ion overspill induced contamination and low plasma density, have plagued the development of several of these deposition approaches.²⁶

The analysis of molecular dynamics simulations of Cu/Co systems indicates that the critical energies for Ar ions needed to overcome flattening energy barriers (normally less than 2 eV) are in the 10 eV range.²⁰ They also show that the critical ion energy for intermixing can be higher, especially if oblique incidence angles are used.²² These simulations suggest several promising deposition possibilities for reducing interfacial roughness and interlayer mixing using low energy ion assistance.^{20,22,27} For example, the simultaneous use of very low ion energies during vapor deposition facilitates the growth of a smooth surface by athermally activating the lateral surface diffusion of the surface atoms. Provided the ion energy is below the (ion mass and ion incident angle dependent) critical energy for intermixing, this can be accomplished without a loss of chemical sharpness across interfaces. This latter issue becomes much less important if ion assistance is delayed during the deposition of a new layer or postponed until layer's deposition is complete. Three approaches for deposition of high quality multilayers therefore appear promising: (i) simultaneous ion assistance with deposition (using very low ion energies at oblique incidence angles), (ii) modulated ion energy assistance (where the ion energy is increased after an interface is buried by several layers of new atoms), and (iii) sequential ion assistance where higher ion energies can be used for flattening after a layer has been deposited.

Here, we experimentally explore the use of these ion assistance strategies to grow a model Ta/Cu bilayer. This system affords good electron scattering contrast in high resolution transmission electron microscopy allowing direct observations of interfacial structures. Copper has also been used extensively as an underlayer (seed layer) in magnetic structures,^{28–31} and for deep submicron interconnects.^{5,6,32} In these applications, copper can easily diffuse into surrounding

silicon structures,³² and so a Ta diffusion barrier layer is frequently used to protect the underlying silicon devices.^{33,34}

Previous simulations of Ta/Cu system by Klaver and Thijssen, indicated existence of mixing and many defects at the interface between Ta and Cu films.³⁵ They also showed consistent roughness development in Cu film deposition on various Ta substrates.^{35,36} Based on this knowledge, we begin by briefly examining molecular dynamics simulation results for the ion assisted growth of Cu on Ta, which show that the system has a similar ion assistance response to the Co/Cu system studies that have been extensively simulated in the past.^{20,22,27} The simulations reconfirm the potential value of the three ion assistance approaches and identify preferred ion energies and flux ratios. A biased target ion beam deposition approach was developed³⁷ to access the simulated process environments and used to deposit Cu/Ta films using the best ion assistance strategies identified by modeling. Transmission electron microscopy is used to characterize the interfacial structures, and electrical resistivity measurements are used to provide insight into the electron scattering defects contained in these bilayers. The results confirm that the very low energy ion assisted growth hypotheses identified by atomistic simulations are practically realizable using the biased target ion beam deposition approach.

II. MOLECULAR DYNAMICS SIMULATIONS OF TA/CU VAPOR DEPOSITION

A. Simulation method

Details of the simulation methodology used to model the low energy ion assisted vapor deposition of multilayer systems can be found in a previous paper.²⁰ It was modified here for the Ta–Cu system by using an initially flat β -Ta substrate crystal created from 12 (100) planes stacked in the x direction, 12 (004) planes in the y (growth) direction, and 12 (0 $\bar{1}$ 0) planes in the z direction. An embedded atom method (EAM) potential was used for the calculation of the interatomic forces between the metal atoms^{18,38,39} and a universal pair potential was used to define the interatomic forces between inert gas (argon) atoms and between metal and inert gas atoms.⁴⁰ Periodic boundary conditions were used in both the x and z directions to minimize the effects of the relatively small crystal size in these two directions. Inert gas ions and adatoms with a prescribed incident angle θ (45° for both gas ions and metal adatoms), and incident kinetic energy E_i (0.5 eV for metal adatoms), were continuously injected toward the surface. To uniquely define a three-dimensional incident direction with a single parameter, θ , it was assumed that the ions were injected in the x - z plane. To avoid a crystal shift during ion/atom impact, the bottom three (004) Ta layers were fixed during the simulations. The two Ta monolayers above the fixed region were kept at a constant temperature of 300 K to create quasi-isothermal growth conditions. Sufficient time (at least 0.15 ps) between (adatom or ion) impacts was used for relaxation and dissipation of the impact energy so that the effects of the impacts could be considered independent. In simultaneous ion assistance method, inert ion energies up to 25 eV and ion:metal flux ratios up to 15 were used to understand the role of ion energy and ion flux

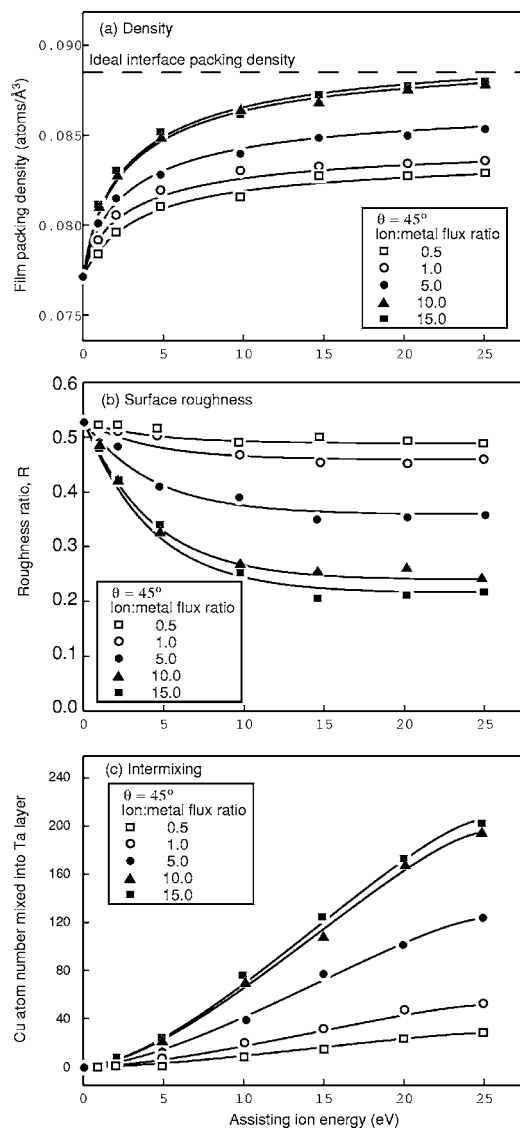


FIG. 1. Molecular dynamics simulation results for Cu films deposited on a Ta buffer layer using a simultaneous ion assistance method: (a) film packing density, (b) surface roughness, and (c) interfacial mixing as a function of assisting argon ion energies at a fixed ion-to-atom flux ratio and an ion incident angle of 45° .

on film properties, while inert ion energies up to 30 eV with fixed ion:metal flux ratio of 6 and ion fluence of $1.0 \text{ ions}/\text{\AA}^2$ were used in modulated energy and sequential ion assistance methods, respectively.

B. Results

The simultaneous ion assistance simulations revealed the formation of a variety of defects at the Cu on Ta interface and within the Cu film. These arose from shadowing effects, atomic exchange across the Cu–Ta interface, and the large lattice constant mismatch (7.6% in minimum) between the (004) β -Ta and (111) fcc Cu. To characterize film's structure, the packing density (which is inversely proportional to the vacancy defect concentration), surface roughness, and the degree of interlayer mixing of the simulated Cu films were calculated and are plotted in Fig. 1 as a function of ion energy and ion:atom flux ratio using an ion incident angle of

45° . To characterize the roughness of the simulated structures, an interfacial roughness parameter R was defined that depended on both the height and the width of surface asperities:⁴¹

$$R = \frac{\sum_{i=1}^n \left(\frac{h_{il} + h_{ir}}{2} \right)}{\sum_{i=1}^n w_i}, \quad (1)$$

where h_{il} and h_{ir} are, respectively, the height measured from the left and right of the i th asperity and w_i is the width of this asperity. Summation is conducted over the n asperities in the x direction.

It can be seen from Figs. 1(a) and 1(b) that when the ion energy and ion/atom flux ratio were both low, the film density was also very low and the film roughness was high. Many adatoms that were deposited on surface asperities remained there, and numerous vacancy-type defects became trapped in the film during its growth. In this regime, the kinetic energy transferred to surface adatoms was insufficient to overcome the Ehrlich-Schwoebel energy barriers at the terrace edges.²⁰ These adatoms then remained adsorbed on a surface asperity without undergoing ion impact induced diffusion. This low energy, low ion:atom flux ratio regime is referred to as the surface adsorption dominated regime. Deposition in the surface adsorption regime was responsible for the growth of structure containing high defect concentrations, low film densities, and rough interfaces.

The film density increased and the surface roughness decreased as the ion energy and ion/atom flux ratio were increased, Figs. 1(a) and 1(b). A relatively high film density and low roughness were obtained for ion energies above 10 eV. At these ion energies, surface adatoms acquired sufficient energy from ion impacts to migrate over the terrace edges and eliminate surface vacancies. Resputtering was found to begin to occur as the ion energy was increased above 30 eV. The most weakly bound surface atoms were preferentially removed, which led to additional smoothing.

Mixing at the interface between the layers increased as the ion/metal flux ratio and the ion energy were increased, Fig. 1(c). For all ion/metal ratios, intermixing was negligible until the ion energy reached a value of 5 eV. Above this ion energy, the mixing probability rose steadily with ion energy. This intermixing became very significant for ion energies above 10 eV and ion/metal flux ratios above 5. Quite low levels of intermixing were observed over the entire ion energy range studied, provided the ion/metal ratio remained below 1.0.

Simulations of modulated energy and sequential ion assistance schemes on the Cu/Ta system revealed very similar results to previous Cu/Co simulations.²⁷ Figure 2 shows film density, surface roughness ratio, and interlayer mixing as a function of argon ion energy. For the modulated energy ion assistance simulations, the first half of the Cu layer was deposited without ion assistance and the remainder was then deposited using the ion energy shown at an ion/metal flux ratio of 6. For the sequential ion assistance simulations, an ion fluence of $1.0 \text{ ions}/\text{\AA}^2$ was applied after completion of deposition of the Cu layer.

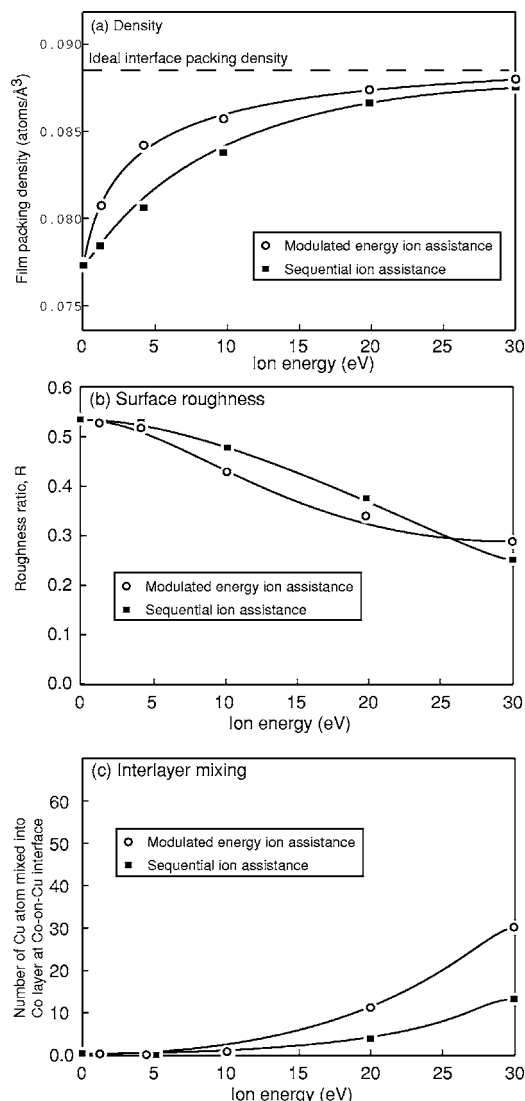


FIG. 2. Simulation results for Cu films deposited on a Ta buffer layer using modulated energy and sequential ion assistance schemes: (a) film packing density, (b) surface roughness, and (c) interfacial mixing and surface roughness as a function of assisting argon ion energies at an ion incident angle of 45° .

Figure 2(a) shows that film's density increased with ion energy for both schemes. The modulated energy ion assistance scheme was marginally superior. It resulted in a slightly higher packing density for most of the simulations. Figures 2(b) and 2(c) show that both approaches resulted in significant surface flattening and very low interlayer mixing even for an ion energy as high as 30 eV. Detailed analysis of simulations indicates that the modulated energy ion assistance method was slightly more effective than the sequential assistance approach because ion assistance was initiated before significant roughening of a surface had developed.

III. EXPERIMENTAL GROWTH APPROACH

A recently developed biased target ion beam deposition^{37,42} (BTIBD) system was used to explore the ion assisted growth of Ta/Cu bilayer films at room temperature. A schematic illustration of the system is shown in Fig. 3. It enables independent control of the assisting ion energy, ion

incident angle, and ion flux. A rotatable target stage on the right side of the chamber accommodated up to six 8 in. metal sputtering targets. The wafer stage on the left faced these sputtering targets. The wafer plane could be tilted so that the adatom and assisting ion incident angles θ could be adjusted from 0° to 90° . The BTIBD system utilized a similar low energy ion source consisting of an end-Hall ion source and a hollow cathode electron source for both sputtering and ion assistance. These ion sources reliably produced a high density, inert gas ion beam with a very low ion energy (in the 0–100 eV range).⁴³ When a negative bias voltage was applied to the sputtering target, the inert gas ions were attracted and made a near normal incidence with the target surface at an easily controlled (but low) energy. During target sputtering, the low sputter yield per ion impact was offset by the use of a high ion current. The near normal incidence for sputtering greatly reduced the creation of energetic neutrals.¹³ The negative bias reduced ion impact with metal tooling, thereby eliminating overspill contamination.¹³

To provide low energy (0–100 eV) ion assistance, the ion assist source was located at the top of the chamber, as shown in Fig. 3. The combination of the end-Hall ion source and a hollow cathode electron beam enabled both the ion energy and ion flux to be independently controlled (by the ion source voltage and current, respectively).⁴³ Experimental studies have indicated that the mean ion energy is approximately 60% of the anode voltage while the ion beam current is approximately 20% of the anode current. The ion flux and energy parameters used below are all derived from these relationships.

Bilayer systems consisting of 5 nm ($\pm 1\%$) of tantalum and 30 nm ($\pm 2\%$) of copper were deposited on 6 in. wafers using the three ion assisting methods (simultaneous deposition with ion assistance, modulated ion energy, and sequential ion assistance) identified by simulations. Each series of experiments used oblique argon ion assistance ($\theta=45^\circ$) during or after metal deposition. The effects of varying the assisting ion beam energy and ion flux were investigated for each of them. For all of the depositions, the base pressure was 3×10^{-8} torr, the Ar working pressure was about 4.5×10^{-4} torr, and the target bias voltage was 300 V.

After deposition, the in-plane sheet resistance of the bilayer system was measured by a four-point probe using a 49-point scan, Prometrix omnimap resistance measurement system. The film texture was characterized using x-ray diffraction (XRD). Surface morphology and roughness were characterized using a tapping mode atomic force microscope (AFM). Film thickness was controlled by the calibrated deposition rate by using x-ray fluorescence (XRF) spectroscopy. It was found that for the deposition conditions used here, the deposition rate for Cu was 0.6 \AA/s while that for Ta growth was 0.2 \AA/s . Auger electron spectrometry (AES) was used to characterize the film composition. The interfacial structures were also characterized by analytical transmission electron microscopy (TEM).

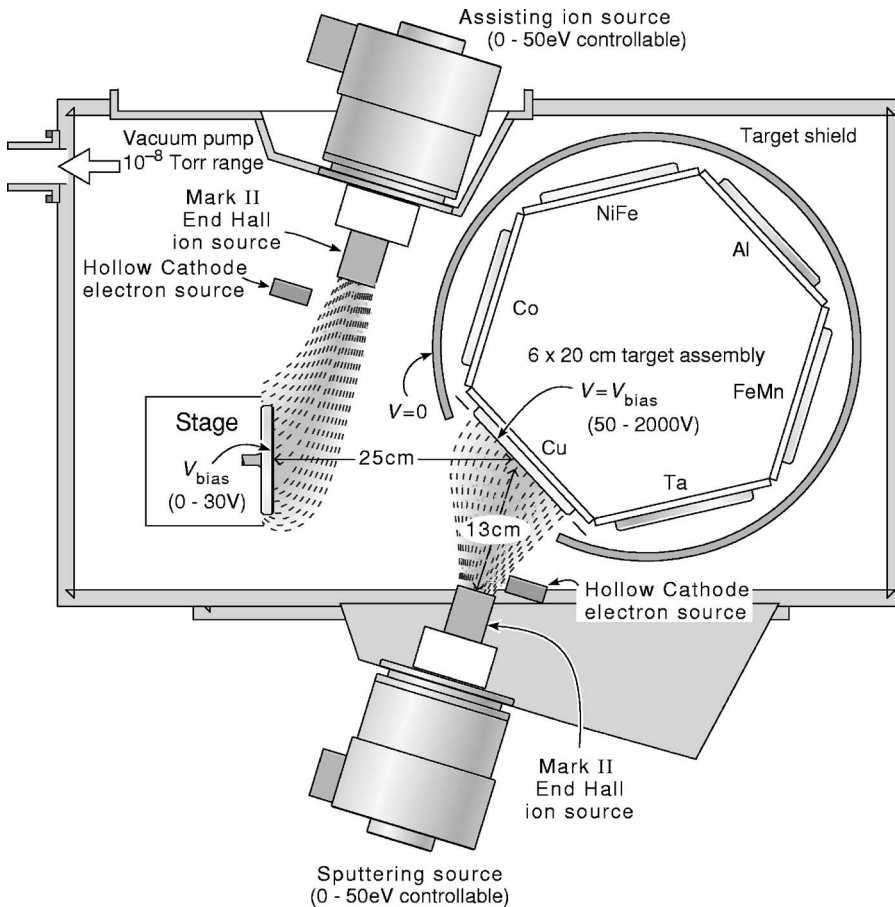


FIG. 3. Schematic illustration of a biased target ion beam deposition system. A high flux, low voltage ion source is used to soft sputter a metal target. A hollow cathode electron source is used to form a low energy ion flux for ion assistance during or after metal deposition. It enables independent control of the ion energy, ion flux, and ion incident angle.

IV. EXPERIMENTAL RESULTS

A. Simultaneous ion assistance

The surface roughness and in-plane electrical resistivity of films grown using simultaneous ion assistance are shown as a function of the assisting ion energy (for an ion-to-atom flux ratio of about 4) in Figs. 4(a) and 4(b). It can be seen that film roughness and especially resistivity are sensitive to the assisting ion energy. The film surface roughness initially decreased as the ion energy was increased from 0 to 7 eV, and then remained constant with further increases in ion energy, Fig. 4(a). These results were in general agreement with simulations, Fig. 1(b). Figure 4(b) shows that the film electrical resistivity at first decreased as the ion energy was increased from 0 to 10 eV but then started to increase as the ion energy was further increased. The electrical resistivity is affected by both the interface (and surface) roughness and the vacancy and impurity atom concentrations in the two layers (i.e., intermixing). The initial drop in resistivity is consistent with a decrease in roughness while the subsequent resistivity rise may be a manifestation of mixing. The solid line in Fig. 4(b) is an interface structure function calculated from a combination of the simulated results (see Appendix for its derivation). It combines the atomic scale features of the structure observed in simulations in a form that approximates their effect on the in-plane electrical resistivity.

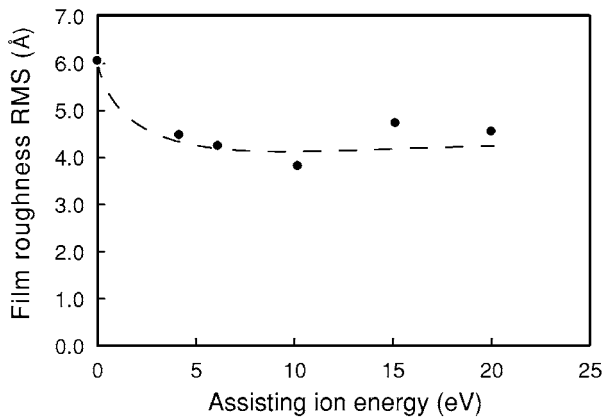
Film roughness and resistivity were also measured as a function of the assisting ion flux using an assisting ion energy of 10 eV. Figure 5(a) shows that an increase of the

ion-to-atom ratio from 0 to 8 results in an $\sim 50\%$ reduction in surface roughness. The roughness then reached a near plateau as the flux ratio was increased above 10. This is again in good agreement with simulation studies [see Fig. 1(b)]. These suggested that at a low ion flux, the assisting ions failed to move many of the adatoms on the surface and led to the accumulation of significant roughness. Simulations also concluded that a significant ion fluence is needed to effectively flatten a surface by direct jumping and exchange mechanisms while still avoiding interlayer mixing [see Fig. 1(c)].

Figure 5(b) shows that the film resistivity initially decreased as the flux ratio was increased to around 6. A further increase in the ion flux then caused an increase in film resistivity. The initial decrease in resistivity is believed to result from impact induced adatom motion which helped to reduce vacancy-type defects, Fig. 1. Again, solid line, which corresponds to simulation predicted structure, captures the trends observed experimentally and will be discussed later.

Further insights into the effect of simultaneous ion beam assistance interfacial structures were obtained from AES measurements of the film composition as a function of depth. Three AES depth profiles were obtained corresponding to deposition with (a) no ion assistance, (b) an ion energy, $E_{\text{ion}}=10$ eV, and a flux ratio of 5, and (c) an ion energy, $E_{\text{ion}}=20$ eV, and a flux ratio of 14, Fig. 6. In the study, the energies for the primary electron beam and the Ar beam used for the AES measurement were 5 and 3 keV, respectively. The data reveal that the sharpest interface was obtained using

(a) Surface roughness



(b) Film resistivity

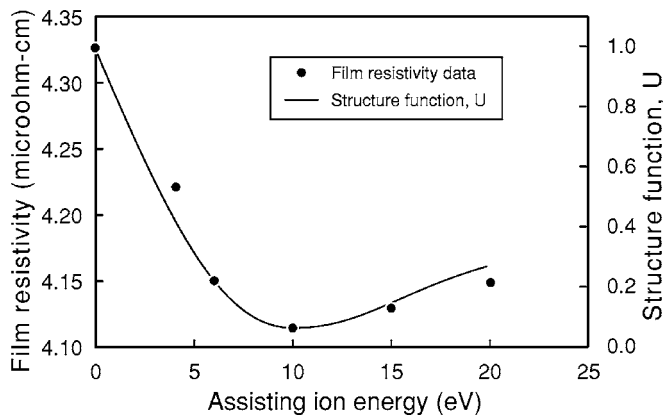
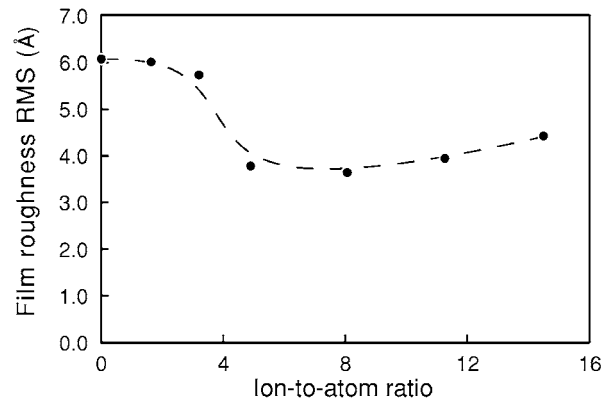


FIG. 4. Cu/Ta film properties as a function of assisting argon ion energy using simultaneous ion beam assisted deposition at an ion-to-atom ratio of 4 and incident angle of 45° : (a) film surface roughness and (b) film electrical resistivity. An empirical structure function U was deduced from simulation results and is shown as the solid curve in (b).

an ion energy of 10 eV and an ion-to-atom ratio of 5. The composition profile of the sample made without ion assistance was slightly wider consistent with interfacial roughness. The samples made using an ion assisting energy of 20 eV and an ion-to-atom ratio of 14 had the most diffuse interface, again consistent with simulation predictions of extensive intermixing during energetic ion assistance treatments.

To further understand interfacial structures, TEM observations for the three samples with (i) no assistance, (ii) ion assistance with medium energy (10 eV) and flux ratio (5), and (iii) ion assistance with higher energy (20 eV) and high flux ratio (14) are shown in Fig. 7. Images were recorded on a JEOL 2010F operated at 200 kV in phase contract mode. The TEM analysis showed that copper had a strong (111) texture regardless of the ion assistance conditions. The Ta texture is harder to determine in the bilayer structure because it is well below the surface and the film thickness is very small [additional samples of single Ta layers were therefore grown using the same deposition conditions. Plain view TEM and x-ray diffraction studies all indicated that Ta films have a β (002) orientation in the growth direction]. Examination of the interfacial structures for the Cu/Ta/Si films grown with no assistance or with high energy and flux ratio

(a) surface roughness



(b) Film resistivity

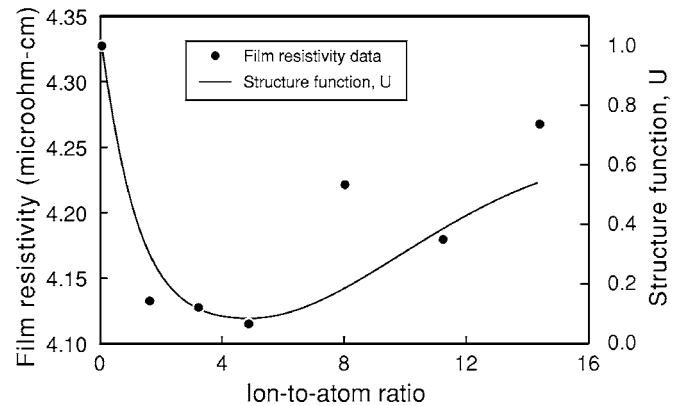


FIG. 5. Cu/Ta film properties as a function of ion-to-atom flux ratio in simultaneous ion beam assisted deposition at an argon ion energy of 10 eV and incident angle of 45° : (a) film surface roughness and (b) film electrical resistivity. Solid line in (b) is for structure function U .

assistance, Figs. 7(a) and 7(c), indicates that they had a more diffused interfacial region than the sample grown with medium energy (10 eV) assistance, Fig. 7(b). We note that Fig. 7(c), in particular, exhibits a highly mixed interface following growth with high energy and high ion flux assistance (while one should consider the possibility that intermixed regions form during the 4 keV Ar^+ milling that is standard in

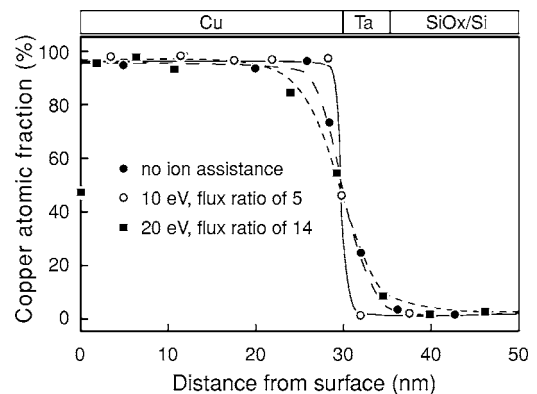


FIG. 6. Measured Auger electron spectrometer depth profiles of composition for Cu/Ta/substrate films deposited using simultaneous argon ion assistance deposition at an incident angle of 45° with three different ion assistance conditions: no ion assistance, 10 eV and ion-to-atom flux ratio of 5, and 20 eV and ion-to-atom flux ratio of 14.

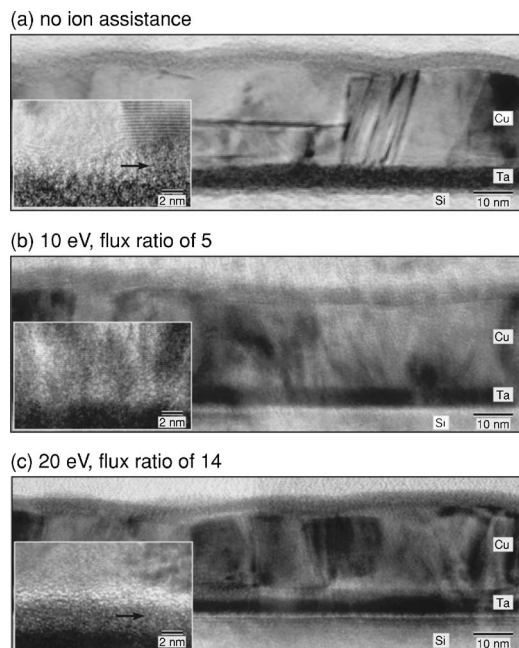


FIG. 7. High resolution TEM cross-section images of the Ta/Cu bilayer interfaces deposited using different simultaneous ion assistance conditions at an incident angle of 45° : (a) no ion assistance, (b) 10 eV and ion-to-atom flux ratio of 5, and (c) 20 eV and ion-to-atom flux ratio of 14. The CuTa region in (c) consists of a heavily mixed solid state solution. Arrow pointed areas are CuTa regions in the figure.

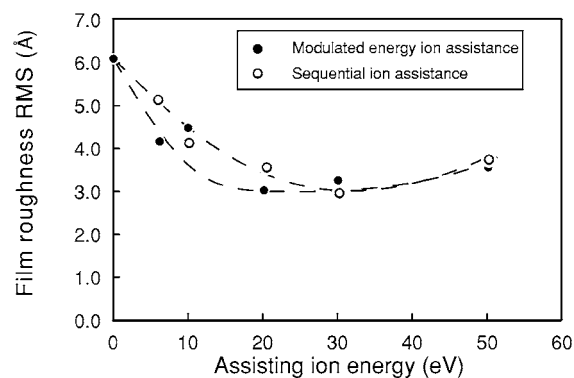
cross-sectional TEM sample preparation, we note that the samples in Figs. 7(a) and 7(c) were prepared under nominally identical conditions).

B. Modulated ion energy and sequential ion beam assistance methods

The modulated ion energy and sequential ion assistance approaches utilized ion assistance only after a layer had been partially or fully deposited. For the modulated ion energy approach, 3 nm of each new layer were first deposited without any ion assistance. The remainder of the layer was then completed using simultaneous ion assistance. The ion-to-metal flux ratio was 6. For the sequential ion assistance experiments, an ion surface modification technique was used after each entire layer had been deposited. The ion current was 0.1 mA and was applied for between 30 and 120 s to the completed tantalum and copper surfaces.

The surface roughness and film electrical resistivity dependencies on ion energy are shown in Figs. 8(a) and 8(b). Both ion assistance methods exhibited similar trends with ion energy. The surface roughness at first decreased significantly as the ion energy was increased from 0 to about ~ 25 eV and then slightly increased for energies above 30 eV. This is again generally consistent with simulation results, Fig. 2(b). Figure 8(b) shows that the film electrical resistivity quickly decreased as the ion energy was increased from 0 to 10 eV. It then remained roughly constant before increasing of ion energy slightly above 30 eV. The resistivity decrease in Fig. 8(b) is consistent with the surface roughness decrease in Fig. 8(a), while the reincrease of resistivity is a

(a) Film surface roughness



(b) Film resistivity

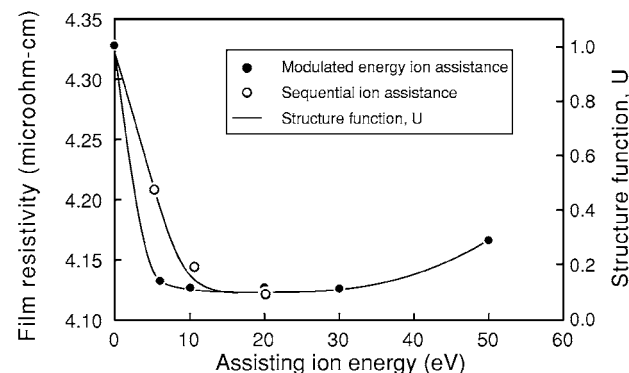


FIG. 8. Cu/Ta bilayer properties as a function of ion energy in modulated ion energy and sequential ion beam treatments: (a) film surface roughness and (b) film electrical resistivity. The ion-to-metal flux ratio was 6 in the modulated ion energy scheme and an ion density of 1 mA/s was applied for about 30 and 120 s to the completed tantalum and copper surfaces, respectively, in the sequential ion assistance.

result of the resputtering mechanism, which is confirmed by AFM studies of film thickness and morphology.

V. DISCUSSION

The atomistic simulations indicate that when low energy argon ions impact Cu or Ta surfaces, they transfer energy to surface atoms, thereby helping them overcome energy barriers and find local minimum energy (more tightly bound) sites. During simultaneous adatom condensation and ion assistance in the 10 eV range, the transferred energy is sufficient to overcome the energy barriers, and flattening occurs frequently enough to suppress the rapid vertical growth of islands and promote step flow growth.^{20,22} The reduced height of local surface asperities in turn minimizes surface shadowing during deposition.

The simulations of ion impacts identify three regimes of assistance. At low ion energies and low ion flux, the surface morphology is determined mainly by adatom adsorption. In this adsorption regime, the size of islands gradually increased during growth since the ion impacts were insufficient to migrate all surface atoms to empty lattice sites. At intermediate ion energy and ion flux, the film growth mode enters a densification regime as vacancy trapping is reduced and flattening starts to become significant. Finally, an intermixing regime occurs at high ion energy and ion flux conditions where significant vertical atom exchange occurs. The adsorp-

tion and densification regimes are responsible for the film surface roughness decrease shown at low ion energy/flux in Figs. 4(a) and 5(a).

Figures 4(b) and 5(b) have shown that the film resistivity decreases as either the ion energy or flux ratio is increased. It eventually reaches a minimum and then increases as the ion energy/flux is further increased. The Cu:Ta resistivity ratio for perfect materials is around 1:60, but the changes observed here had fixed film thickness and were not the result of variations in the Cu/Ta fraction of the film. Furthermore, in our studies only the in-plane resistance was measured and it can be assumed that almost all the current flowed through only the (top) Cu layer. The measured resistivity is therefore a function of Cu layer's structural properties.

Many studies^{44,45} have shown that the resistivity of thin films is a sensitive indicator of the concentration of defects,⁴⁶ such as vacancies and voids, and to the presence of impurity atoms⁴⁷ like those introduced by intermixing at film interfaces. Surface and interfacial roughness can also contribute to increases in resistivity.⁴⁷⁻⁵¹ It is therefore anticipated that the resistivity changes observed in the experiments are related to changes in surface (and interfacial) roughness, film's packing density (vacancy and void content), and alloy scattering due to interlayer mixing. All were evident in the simulations and their combination reached a minimum at about the same ion energy where we observed a minimum for the resistivity.

The resistivity of a layer containing several different electron scattering defects can be estimated by combining models for electron scattering from the surfaces, vacancy-type defects, and impurities (see Appendix). The resulting "structure function" combines these structural parameters in a similar functional form to their effect on the resistivity and is given by

$$U = A \left[1 - \frac{\lambda_e \operatorname{erf}(4\pi h/\lambda_e)}{8\sqrt{\pi}h} \right] + Bn_i + C\delta \tanh\left(\frac{\Delta}{2\delta}\right), \quad (2)$$

where h is the surface roughness, n_i is the vacancy defect concentration, δ is the intermixing zone width, Δ is the film thickness related parameter, λ_e is the Fermi wavelength, A , B , and C are fittable constants, and erf is the error function. The values of this U function with substitution of all the structure parameters deduced from the simulations (Fig. 1) are plotted as the solid lines in Figs. 4(b) and 5(b) using a normalized scale. It can be seen that the trend of U with ion energy and flux matches well the experimental resistivity observations.

Comparison between Figs. 4 and 8 indicates that the ion energy required to flatten a surface using either the sequential or modulated ion energy ion treatments is higher than that needed using the simultaneous ion assistance approach (7 vs 20–30 eV). This arises because during the sequential and (to a lesser extent) modulated energy approaches, significant roughness developed prior to the ion irradiation. This roughness then required relatively high ion energy fluxes to achieve smoothing.²⁷ These higher energy ion treatments are, however, less likely to cause interlayer mixing because the interface was located well below the surface, Fig. 2. Simulations have previously indicated that interlayer mixing in

thin multilayer films can be significantly suppressed by even just a few atomic layers of new material.²⁷ The resulting resistivity and structure function, U , changes in Fig. 8 in the 10–30 eV ion energy range are smaller in the sequential or modulated ion energy assistance approaches than those encountered with simultaneous ion assistance. When the ion beam energy became too high, significant resputtering did occur (the sputtering threshold energy for copper is approximately 20 eV). This resulted in both an increase in the film surface roughness and the film resistivity at ion energies around 50 eV [the sputtering yield of copper is 1% per incident ion at an argon ion energy of 50 eV (Ref. 12)], Fig. 8.

VI. CONCLUSIONS

Low energy ion assisted vapor deposition of Ta/Cu bilayer films was explored using both experimental and simulation approaches. Low energy argon ion impacts were found to significantly affect film structures and electrical properties. The following have been found.

- (1) During simultaneous ion beam assistance with metal deposition, film roughness and resistivity at first decrease as the ion energy/flux ratio increases. The use of ion energies around 10 eV and an ion flux ratio around 6 optimizes film structure properties. Further increases of the ion energy or flux ratio again increase film resistivity by inducing intermixing at the Cu/Ta interface.
- (2) AES and TEM studies have confirmed simulation results and indicate that the interface between Ta and Cu films is (i) nonplanar due to physical roughness when films are grown with no ion assistance and (ii) heavily intermixed when the ion energy and ion flux were high. The sharpest interfaces were achieved at intermediate ion energy and ion flux.
- (3) A structure function that combines the simulated atomic scale structure of a thin film in a way that represents their effect on resistivity is found to account well for experimental variations of film resistivity with ion energy and flux ratio.
- (4) The ion energy for minimum roughness in modulated ion energy and sequential ion assistance was found to be higher than that of a simultaneous ion assistance approach because the islands formed in the latter approaches are on average larger. However, the use of these higher ion energies in these two schemes is less likely to introduce mixing between the layers.
- (5) Significant resputtering at an ion energy above 40 eV appears to be responsible for increases in roughness and resistivity when higher ion energy assisted deposition conditions are used.

ACKNOWLEDGMENTS

We are grateful to the Defense Advanced Research Projects Agency and Office of Naval Research for support of this work under ONR Grant No. N00014-03-C-0288 monitored by Dr. Carey Schwartz and Dr. Julie Christodoulou. We are also grateful for the support of TEM facility by the Office

of Naval Research (Chagaan Baatar, program manager) through ONR Grant No. N000140211039.

APPENDIX: MULTILAYER RESISTIVITY

The resistivity of vapor deposited multilayers is expected to be higher than that of perfectly bonded, flat slabs of the various constituent layers because of electron scattering at rough surfaces, by vacancies, voids, dislocations, and other stacking defects in each layer, and by electron-impurity scattering resulting from interdiffusion between the layers. In the Ta/Cu bilayer system studied here, the resistivities of Ta are much greater than that of Cu (180 and 3 $\mu\Omega$ cm, respectively). In the case of our in-plane resistance measurements, the flow of current can be assumed to be only in the top Cu layer considering the big differences between their resistivities ($\rho_{\text{Cu}}:\rho_{\text{Ta}}=1:60$) and thicknesses ($d_{\text{Cu}}:d_{\text{Ta}}=6:1$). The changes in resistivity measured experimentally are therefore dominated by changes in electron scattering in the Cu layer. Matthiessen's rule then provides a simple means for combining the many electron scattering mechanisms in the film to estimate its electrical resistivity.⁵² The resistivity ρ_F of a thin film in which electrons are scattered within the bulk lattice and at the surface obeys this rule:⁵² $\rho_F=\rho_S+\rho_B$, where ρ_S is the resistivity induced by electron-surface scattering and ρ_B is the bulk resistivity. In vapor deposited multilayers, other scattering mechanisms contribute to the resistivity and in this case the resistivity can be approximated as $\rho_F=\rho_S+\rho_B+\rho_{\text{int}}+\rho_{\text{def}}$, where ρ_{def} is the resistivity induced by lattice defects (e.g., vacancies) and ρ_{int} is the resistivity induced by imperfections at the interface. If it is assumed that the perfect bulk lattice resistivity is constant in the experiments conducted here, then ρ_B can be ignored in consideration of resistivity changes. It is then possible to define a structure-dependent function U to describe resistivity changes in vapor deposited films,

$$U = \rho_S + \rho_{\text{int}} + \rho_{\text{def}}. \quad (\text{A1})$$

The Fuchs-Schodheimer model can be used to describe the scattering of electrons at the surface of a thin film. In this model, a specular coefficient p is used to describe a fraction of the electrons that are scattered elastically at the solid surface. The resistivity ratio of film ρ_f to that of the bulk metal ρ_0 is then described by^{48,51}

$$\frac{\rho_f}{\rho_0} = \frac{\Phi_p(k)}{k}, \quad (\text{A2})$$

where

$$\frac{1}{\Phi_p(k)} = \frac{1}{k} - \frac{3}{2k^2}(1-p) \int_0^\infty \left(\frac{1}{t^3} - \frac{1}{t^5} \right) \frac{1-e^{-kt}}{1-pe^{-kt}} dt, \quad (\text{A3})$$

and k is the ratio of film thickness to the bulk solid electron mean free path. Here p is a function of the electron incident angle relative to the surface normal, θ :⁵³

$$p = \exp[-(4\pi\gamma)^2 u^2], \quad (\text{A4})$$

where $\gamma=h/\lambda_e$, h is the surface roughness, λ_e is the Fermi wavelength, and $u=\cos\theta$. In the case of large k , Eq. (A2) has the approximate form

$$\frac{\rho_f}{\rho_0} = \int_0^1 du \left[1 + \frac{3}{8k}(1-p) \right]. \quad (\text{A5})$$

The surface induced resistivity can then be written as

$$\rho_S = \int_0^1 du \left[\frac{3\rho_0}{8k}(1-p) \right]. \quad (\text{A6})$$

The resistivity induced by scattering of defects (vacancies and impurities) within the film can be expressed as⁵⁴

$$\rho_{\text{def}} = \frac{n_0\tau_0}{\sigma_0 n(d)\tau(d)}, \quad (\text{A7})$$

where $\sigma_0=n_0e^2\tau_0/m^*$ (m^* is the carrier effective mass) is the Drude conductivity, $n(d)$ is the average density of electrons, and $1/\tau(d)=2\pi U_0^2 n_i g(\epsilon_F) m$ (U_0 is the strength of impurity potential, $g(\epsilon_F)$ is the density of state, n_i is the defect density, and m is the coefficient related to density function). Therefore, Eq. (A6) becomes

$$\rho_{\text{def}} = \frac{2\pi U_0^2 n_i g(\epsilon_F) m m^*}{n(d)e^2}. \quad (\text{A8})$$

To account for interdiffusional effects on the resistivity near an interface between dissimilar materials, Skomski *et al.*⁴⁷ have proposed a phenomenological expression in the thick film limit as

$$\rho_{\text{int}} = \frac{2\delta\rho_M}{\Delta} \tanh\left(\frac{\Delta}{2\delta}\right), \quad (\text{A9})$$

where Δ is a film thickness related parameter and ρ_M is the resistivity of an intermixed interfacial region of width 2δ that exists between films a and b. The structure function U can then be expressed as a combination of Eqs. (A6), (A8), and (A9):

$$U = \int_0^1 du \left[\frac{3\rho_0}{8k}(1-p) \right] + \frac{2\pi U_0^2 n_i g(\epsilon_F) m m^*}{n(d)e^2} + \frac{2\delta\rho_M}{\Delta} \tanh\left(\frac{\Delta}{2\delta}\right). \quad (\text{A10})$$

If the film resistivity is assumed to be only a function of the surface root mean square roughness h vacancy concentration n_i and interdiffusion width δ , and all other contributions remain constant, then the change in resistivity of a bilayer thin film (consisting of a good conductor on top of a poor one) can be approximated by

$$U = A \left[1 - \frac{\lambda_e \operatorname{erf}(4\pi h/\lambda_e)}{8\sqrt{\pi}h} \right] + B n_i + C \delta \tanh\left(\frac{\Delta}{2\delta}\right), \quad (\text{A11})$$

where A , B , and C are constants to be fitted, and erf is an error function.

¹S. M. Rossnagel, J. Vac. Sci. Technol. A **21**, S74 (2003).

²S. Honda, S. Ohmoto, R. Imada, and M. Nawate, J. Magn. Magn. Mater. **126**, 419 (1993).

³D. M. C. Nicholson, W. H. Butler, X. G. Zhang, J. M. Maclaren, B. A. Gurney, and V. S. Speriosu, J. Appl. Phys. **76**, 6805 (1994).

⁴A. K. Petford-Long, D. J. Larson, A. Cerezo, X. Portier, P. Shang, D.

- Ozkaya, T. Long, and P. H. Clifton, *Microsc. Microanal.* **10**, 366 (2004).
- ⁵C. K. Hu, B. Luther, F. B. Kaufman, J. Hummel, C. Uzoh, and D. J. Pearson, *Thin Solid Films* **262**, 84 (1995).
- ⁶S. P. Murarka, R. J. Gutmann, A. E. Kaloyeros, and W. A. Lanford, *Thin Solid Films* **236**, 257 (1993).
- ⁷J. K. Hirvonen, *Mater. Sci. Rep.* **6**, 215 (1991).
- ⁸J. S. Colligon, H. Kheyrandish, G. Carter, and M. C. Simmonds, *Vacuum* **46**, 919 (1995).
- ⁹P. D. Horak and U. J. Gibson, *Appl. Phys. Lett.* **65**, 968 (1994).
- ¹⁰D. F. Grogan, T. Zhao, B. G. Bovard, and H. A. Macleod, *Appl. Opt.* **31**, 1483 (1992).
- ¹¹T. J. Whetten, A. A. Armstead, T. A. Grzybowski, and A. L. Ruoff, *J. Vac. Sci. Technol. A* **2**, 477 (1984).
- ¹²S. Savas, R. George, D. Gilbert, J. Cain, M. Herrick, A. Nagy, and K. Karuppana, *Micro* **22**, 61 (2004).
- ¹³X. W. Zhou, H. N. G. Wadley, and S. Sainathan, *Nucl. Instrum. Methods Phys. Res. B* **234**, 441 (2005).
- ¹⁴I. Petrov, L. Hultman, U. Helmersson, J. E. Sundgren, and J. E. Greene, *Thin Solid Films* **169**, 299 (1989).
- ¹⁵B. Q. Chen, F. J. Wang, Y. K. Wang, J. X. Wang, H. M. Han, C. N. Wang, T. Y. Niu, and H. W. Gao, *Scr. Metall.* **22**, 757 (1988).
- ¹⁶T. Lin, K. Y. Ahn, J. M. E. Harper, P. B. Madakson, and P. M. Fryer, *Thin Solid Films* **154**, 81 (1987).
- ¹⁷X. W. Zhou and H. N. G. Wadley, *J. Appl. Phys.* **87**, 8487 (2000).
- ¹⁸X. W. Zhou *et al.*, *Acta Mater.* **49**, 4005 (2001).
- ¹⁹W. Zou, H. N. G. Wadley, X. W. Zhou, R. A. Johnson, and D. Brownell, *Phys. Rev. B* **64**, 174418 (2001).
- ²⁰J. J. Quan, X. W. Zhou, and H. N. G. Wadley, *Surf. Sci.* **600**, 2275 (2006).
- ²¹X. W. Zhou and H. N. G. Wadley, *J. Appl. Phys.* **90**, 3359 (2001).
- ²²J. J. Quan, X. W. Zhou, and H. N. G. Wadley, *Surf. Sci.* **600**, 4537 (2006).
- ²³X. Portier and A. K. Petford-Long, *J. Phys. III* **32**, R89 (1999).
- ²⁴K. W. Kwon, H. J. Lee, and R. Sinclair, *Appl. Phys. Lett.* **75**, 935 (1999).
- ²⁵A. J. Devasahayam, J. C. S. Kools, C. C. Hu, M. Mao, C. L. Lee, W. Skinner, and J. Hautala, *IEEE Trans. Magn.* **40**, 2200 (2004).
- ²⁶X. W. Zhou, H. N. G. Wadley, and W. H. Butler (unpublished).
- ²⁷J. J. Quan, X. W. Zhou, and H. N. G. Wadley, *J. Cryst. Growth* (to be published).
- ²⁸S. Bae, N. Matsushita, S. Zurn, L. Sheppard, E. J. Torok, and J. H. Judy, *IEEE Trans. Magn.* **36**, 2850 (2000).
- ²⁹D. Wang, J. M. Daughton, K. Bussmann, and G. A. Prinz, *J. Appl. Phys.* **83**, 7034 (1998).
- ³⁰K. Bussmann, S. F. Cheng, G. A. Prinz, Y. Hu, R. Gutmann, D. Wang, R. Beech, and J. Zhu, *IEEE Trans. Magn.* **34**, 924 (1998).
- ³¹K. Bussmann, G. A. Prinz, S. F. Cheng, and D. Wang, *Appl. Phys. Lett.* **75**, 2476 (1999).
- ³²S. P. Murarka and S. W. Hymes, *Crit. Rev. Solid State Mater. Sci.* **20**, 87 (1995).
- ³³K. Holloway and P. M. Fryer, *Appl. Phys. Lett.* **57**, 1736 (1990).
- ³⁴K. V. Kwon, C. Ryu, R. Sinclair, and S. S. Wong, *Appl. Phys. Lett.* **71**, 3069 (1997).
- ³⁵T. P. C. Klaver and B. J. Thijsse, *Mater. Res. Soc. Symp. Proc.* **721**, 37 (2002).
- ³⁶T. P. C. Klaver and B. J. Thijsse, *J. Comput.-Aided Mater. Des.* **10**, 61 (2003).
- ³⁷H. N. G. Wadley, X. W. Zhou, and J. J. Quan, *Biased Target Ion Beam Deposition of Spin-Valves* in Proceedings of the Non-Volatile Memory Technology Symposium, San Diego, 2003, pp. 12-1 to 12-8.
- ³⁸R. A. Johnson, *Phys. Rev. B* **39**, 12554 (1989).
- ³⁹X. W. Zhou, R. A. Johnson, and H. N. G. Wadley, *Phys. Rev. B* **69**, 144113 (2004).
- ⁴⁰R. E. Johnson, *Energetic Charged-Particle Interactions with Atmospheres and Surfaces* (Springer-Verlag, 1990), Vol. 19.
- ⁴¹X. W. Zhou and H. N. G. Wadley, *J. Appl. Phys.* **84**, 2301 (1998).
- ⁴²V. V. Zhurin, H. R. Kaufman, J. R. Kahn, and T. L. Hylton, *J. Vac. Sci. Technol. A* **18**, 37 (2000).
- ⁴³H. R. Kaufman, R. S. Robinson, and R. I. Seddon, *J. Vac. Sci. Technol. A* **5**, 2081 (1987).
- ⁴⁴J. Barnas and Y. Bruynseraede, *Phys. Rev. B* **53**, 5449 (1996).
- ⁴⁵W. Wang, R. F. Huang, L. S. Wen, L. P. Guo, and W. K. Wang, *J. Mater. Sci.* **15**, 75 (1999).
- ⁴⁶S. K. Choi and J. I. Lee, *J. Vac. Sci. Technol. A* **19**, 2043 (2001).
- ⁴⁷R. Skomski, M. Enrech, and J. M. D. Coey, *Nanostruct. Mater.* **1**, 337 (1992).
- ⁴⁸K. Fuchs, *Proc. Cambridge Philos. Soc.* **34**, 100 (1938).
- ⁴⁹A. Misra, M. F. Hundley, D. Hristova, H. Kung, T. E. Mitchell, M. Nastasi, and J. D. Embury, *J. Appl. Phys.* **85**, 302 (1999).
- ⁵⁰R. C. Munoz, C. Arenas, G. Kremer, and L. Moraga, *J. Phys.: Condens. Matter* **15**, L177 (2003).
- ⁵¹E. H. Sondheimer, *Adv. Phys.* **1**, 1 (1952).
- ⁵²J. Bass, *Adv. Phys.* **21**, 431 (1972).
- ⁵³S. B. Soffer, *J. Appl. Phys.* **38**, 1710 (1967).
- ⁵⁴N. Trivedi and N. W. Ashcroft, *Phys. Rev. B* **38**, 12298 (1988).